PERGAMON

Available online at www.sciencedirect.com

SCIENCE DIRECT®

Applied Thermal Engineering 23 (2003) 779–795

APPLIED THERMAL ENGINEERING

www.elsevier.com/locate/apthermeng

Computational analysis of temperature rise phenomena in electric induction motors

Ying Huai [a], Roderick V.N. Melnik [b,*], Paul B. Thogersen [c]

[a] *Technical University of Darmstadt, Energie- und Kraftwerkstechnik, Petersenstraße 30, 64287 Darmstadt, Germany*
[b] *Faculty of Science and Engineering, Mads Clausen Institute, University of Southern Denmark, Grundvigs Alle 150, Sonderborg, DK-6400, Denmark*
[c] *Danfoss Drives A/S, Denmark*

Received 12 October 2002; accepted 20 December 2002

Abstract

In developing electric machines in general, and induction motors in particular, temperature limits is a key factor affecting the efficiency of the overall design. Since conventional loading of induction motors is often expensive, the estimation of temperature rise by tools of mathematical modelling and computational experiments becomes increasingly important. In the present paper we develop and validate experimentally a model accounting for losses and describing thermal phenomena in induction motors. The developed model has been implemented in FEMLAB, and has been applied to predict temperature rise in totally enclosed fan-cooled induction motors. Comparisons with experimental results obtained with a 1.5 kW standard squirrel-cage induction motor show the effectiveness of the developed model in predicting temperature rise for a range of operating conditions, in particular for different frequencies and voltages. Finally, a SIMULINK-based control loop has been developed by using the thermal model as an input.
© 2003 Elsevier Science Ltd. All rights reserved.

Keywords: Electric induction motor; Thermal model; Finite element analysis frequency

1. Introduction

An electric machine is a complex engineering system that consists of different materials with different thermal properties and distributed heat sources. Although we witness advances achieved

* Corresponding author. Tel.: +45-6550-1681; fax: +45-6550-1660.
E-mail address: rmelnik@mci.sdu.dk (R.V.N. Melnik).

1359-4311/03/$ - see front matter © 2003 Elsevier Science Ltd. All rights reserved.
doi:10.1016/S1359-4311(03)00013-9

in many aspects of electric machine design, it is generally agreed that the development of thermal design methodologies for electric machines lags behind [3].

One of the most common AC machines found in industrial applications is the three-phase cage induction machine of totally enclosed fan-cooled (TEFC) design. These motors are often driven by variable-voltage and variable-frequency inverters. As a result, we can achieve variable speeds and the torque control of particular loads, but the pay-off for that will be an increase in operating temperature conditions of the motor. Moreover, it is well known that a high temperature is one of the sources of increased stress on induction motors' insulation system. Recognising the importance of the thermal factor in the overall effectiveness of motor design, different techniques have been proposed for thermal monitoring, in particular those related to rotor and stator temperature [2]. Most of such techniques are based on some intermediate estimates, e.g. the rotor resistance identification [2], but in using such techniques little can be said about the distribution of temperature and the identification of thermally critical parts of the motor under the given operating conditions.

The thermal analysis of electric induction motors can supplement effectively thermal monitoring techniques, contributing substantially to a better understanding of the overall performance and prevention of failures of these electric machines. In this paper we develop a mathematical model allowing one to calculate the distribution of motor temperature as a function of input parameters determined by the current operating conditions, implement the model, and compare the results of computations with the results of experimental measurements. The model can be applied for various frequencies and loads, and the identified temperature can then be compared to thermal limits and alarm thresholds to prevent motors from overheating which could be generated by a range of factors, e.g. overload, locked rotor, prolonged starts, or unbalanced current to name just a few.

The methodology based on numerical techniques such as finite differences and finite elements has become an important tool in the thermal analysis of electric machines (e.g., [1,6,20]). Although the methodology offers more flexibility and higher accuracy compared to more traditional engineering approaches such as the lumped and distributed parameter method [9,14,17,18], its application has often been limited to simplified geometries and steady-state analysis due to a high geometrical and computational complexity of the problem. Simplified methodologies, in particular those based on theory of thermal networks, are quite useful in the preliminary analysis. In using such methodologies, the electric machine is subdivided into elements which are treated as nodes on a circuit network, while the thermal capacitances are considered to be lumped at each node and thermal resistances are introduced between two consecutive nodes. To achieve a sufficiently accurate result, a very large number of nodes on a network is typically needed, and therefore technically the procedure becomes much similar to the numerical discretisation of the motor geometry. However, it is important to emphasize that the flexibility of thermal-network-based models will lessen when the motor works in different situations because it is difficult to calculate the rate of heat addition to each node and thermal resistances between two nodes. Different empirical thermal models have also been proposed in the literature (e.g., [4]). Typically, such models provide estimates for stator and rotor temperatures by using lumped-parameter thermal models. A typical assumptions used in this approach are related to a single frequency-dependent thermal resistance and time constant. In practice, however, stator and rotor have different values of thermal resistance and capacitance, and hence the procedure has to be sub-

stantially modified virtually on a case-to-case basis. In the meantime, efficient graphical user interfaces, automatic mesh generation procedures, visualization, and post processing, intrinsic to the finite element analysis, provide a general tool for the thermal analysis of electric induction motors.

The paper is organized as following: In Section 2 we present a general mathematical model for estimating thermal characteristics of electric motors. This is followed by a detailed analysis of power loss models, schemes for modelling heat sources and heat transfer phenomena in different parts of the electric motor. The model implementation procedure is described in Section 3. Section 4 is devoted to the model validation, and a model application example is discussed in Section 5.

2. Mathematical model for thermal analysis of electric induction motors

We base our consideration on the following energy balance model:

$$\rho\left(\frac{\partial e}{\partial t}+\mathbf{v}\cdot\nabla e\right)=\boldsymbol{\sigma}:\boldsymbol{\epsilon}-\nabla\cdot\mathbf{q}+\rho Q, \tag{1}$$

where ρ is the density of the material, e is the internal energy, $\mathbf{q}$ is the energy flux, $\boldsymbol{\epsilon}$ and $\boldsymbol{\sigma}$ are deformation and stress tensors, respectively, Q is the energy supply. We can reduce (1) to the following form (e.g., [11])

$$\rho\frac{\partial e}{\partial t}+\nabla\cdot\mathbf{q}=\widetilde{Q}, \tag{2}$$

where $\widetilde{Q}=\rho Q+\boldsymbol{\sigma}^{\mathrm{T}}:(\nabla\mathbf{v})$ accounts for the energy supply and changes in the internal energy due to different types of losses, e.g. friction and cooling losses, and electromagnetic losses. Assuming that the internal energy can be expressed as $e=e(\theta)$, we have that

$$\mathrm{d}e/\mathrm{d}t=c_v\mathrm{d}\theta/\mathrm{d}t \quad \text{where} \quad c_v=\mathrm{d}e/\mathrm{d}\theta, \tag{3}$$

where c_v is the specific heat at constant volume. Model (1)–(3) is supplemented by boundary and initial conditions. Depending on the part of the motor under consideration we use Dirichlet's, Neumann's, specified flux, or radiation boundary conditions. In doing so, we use Fourier's law $\mathbf{q}=-k\nabla T$, Newton's law of cooling/heating accounting for convection from the surface $Q_1=h(T_{\mathrm{ext}}-T)$ (heat acquired from the surrounding), and the Stefan–Bolzmann law giving the radiative energy net exchange $Q_2=C_{\mathrm{cons}}(T_{\mathrm{am}}^4-T^4)$ (heat acquired due to the incoming radiation), where h is the convection coefficient, T_{ext} and T_{am} are external and ambient temperatures, respectively, k is the thermal conductivity coefficient, and C_{cons} is the radiative transfer coefficient. We follow [15] in developing a general representation of boundary conditions for the problem. In this context, it is convenient to introduce a scalar quantity, W_{out}, representing heat losses at the surface. Then, the energy balance at the surface [15] is defined by the formula

$$W_{\mathrm{out}}\equiv q_{\mathrm{sup}}=k\nabla T-h(T_{\mathrm{ext}}-T)-C_{\mathrm{cons}}(T_{\mathrm{am}}^4-T^4). \tag{4}$$

The representation (4) allows us to "activate" coefficients k, h, C_{cons} depending on which specific type of heat transfer (conductive, radiative, or convective) should be accounted for in a particular part of the motor. If we denote the heat generated within the system by W_{in} then the original model

can be schematically reformulated as a basic conservation law in the form $W_{out} = W_{in} - W_{change}$ where $W_{change} = \rho c_v \partial T/\partial t$ would formally represent the change in energy stored within the system. In order to complete the model formulation we need to specify functions and coefficients entering the model (1)–(4) since they depend on the geometry and nature of the region of the motor and/or the boundary segment under consideration.

2.1. Power losses in induction motors: heat sources modelling

It is well known that experimental techniques aiming at determining total losses and temperature rise in electric induction motors may be expensive, and their effectiveness is often limited to specific types of motors (e.g., [12,13]). It is, therefore, often important to estimate analytically or numerically power losses in the motor in order to use the estimates obtained as input parameters for thermal modelling (e.g., [3]).

Before moving further in modelling heat sources, we shall briefly describe the fundamentals of the motor we consider in this paper. In Fig. 1 we present a basic structure of a TEFC induction motor that is analysed. As the name suggest, in such motors AC voltages are induced in the rotor circuit by the rotating magnetic field of the stator. When three-phase balanced and symmetric currents are applied to the stator winding, a rotating magnetic flux is produced in the air gap. If the frequency of the applied currents is known, say f, then the speed of the rotating magnetic flux, n_s, can be calculated (in revolutions per minute, rpm) as

$$n_s = 120f/p, \tag{5}$$

where p is the number of poles per phase. The rotating flux in the air gap will induce voltage in the rotor winding, and a current flow in the rotor winding (since the rotor winding circuits are closed). Then, the classical scheme applies: the current in the rotor winding will interact with the rotating magnetic field in the air gap, and a Lorentz force will be produced and act on rotor conductors $\mathbf{F} = q\mathbf{v} \times \mathbf{B}$, where q is a charge moving through an external magnetic field $\mathbf{B}$ with velocity $\mathbf{v}$. As a

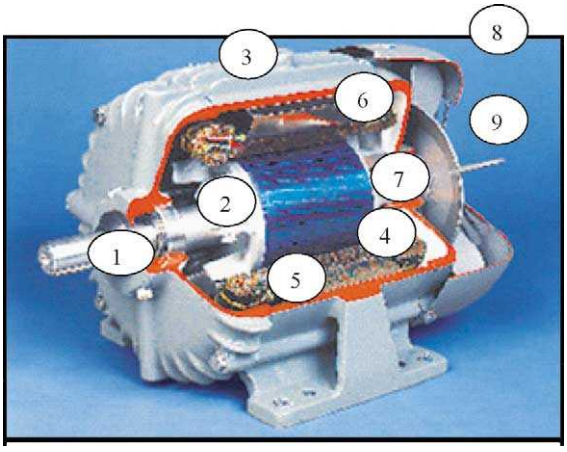

Fig. 1. The structure of a TEFC squirrel-cage induction motor. (1) Shaft; (2) bearing; (3) frame; (4) stator coil; (5) end winding; (6) stator core; (7) rotor; (8) end cap; (9) fan.

result of this force, a torque is produced and the rotor assembly starts rotating. As it is well known, the requirement for the torque to be produced in the motor the actual mechanical rotating speed of the rotor should be less than the speed of the rotating magnetic flux produced by the stator. The difference in rotating speeds between the stator produced magnetic flux and the rotor is measured by the slip

$$s = n_s - n/n_s, \tag{6}$$

where n is the rotor speed in rpm. When a motor is used to drive the load connected on its shaft, it inevitably encounters losses, which serve as heat sources distributed throughout the whole motor and vary with different operating conditions. To account for the total losses is an extremely difficult task, but it is possible to divide all motor power losses into five major categories:

- stator core losses (iron losses, denoted further by P_m);
- stator coil losses (copper losses, denoted further by P_{cu1});
- rotor coil losses (copper losses, denoted further by P_{cu1});
- friction and windage losses (mechanical losses);
- stray load losses.

Given the supply frequency, ω, it is possible to approximate the power losses by experimentally fitted dependency

$$P_{losses} = F(\omega), \tag{7}$$

where it is often appropriate to use a cubic polynomial in place of F, e.g. $P_{losses} = a_0 + a_1\omega + a_2\omega^2 + a_3\omega^3$. However, it is important to emphasize that the distribution of losses in different parts of the motor could be substantially different. Therefore, in the general case approximation (7) has to be replaced by a more rigorous technique for the evaluation of power losses.

The estimates of friction losses usually account for a small part of the total losses, but when the speed increases, their contribution should be included, in particular in the air gap, end rings, rotor ends, shaft and bearing. The estimates of these losses as well as cooling losses are made in the way described in detail in [18]. It is known that the first three categories of losses mentioned above (generically known as electromagnetic losses) account for 75–90% percent of the overall losses. Therefore, in what follows we focus on the evaluation of these electromagnetic losses which can contribute substantially to the temperature distribution in the motor.

Different methodologies exist to deal with different aspects related to the electromagnetic losses evaluation. For example, the coupled circuit methodology [10] seems to be particularly effective when a quite detailed analysis of the winding under different conditions is required (see also [21]). Here, we use a more classical approach based on the equivalent circuit methodology (e.g., [4,5,22]. The induction motor equivalent circuit model, shown in Fig. 2, is constructed by using the following set of induction motor parameters: $(R_1, X_{1\sigma})$, (R_m, X_m), and $(R_2, X_{2\sigma})$. Each pair represents resistance and leakage reactance, respectively. The first pair deals with the stator parameters, while the third one deals with the rotor. The second pair of parameters takes care of magnetising effects, and models the generation of the air gap flux within the induction motor. The importance of this pair increases when the induction motor is driven with voltages other than the rated supply

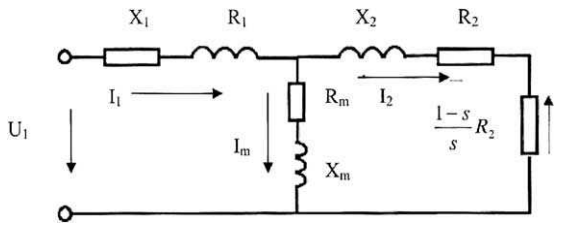

Fig. 2. The equivalent circuit of an induction motor used in calculation of losses.

voltage and frequency due to the fact that under operation with a variable voltage and/or variable frequency the induction motor could saturate if the stator voltage is excessively large. Other parameters of interest presented in Fig. 2 are U_1 (per-phase supply voltage of the stator) and I_1, I_m, I_2 (the phase currents of stator, magnetising and rotor circuit, respectively). These parameters can vary in the model with different operational conditions. By using the standard equivalent scheme technique, we apply Ohm's law and calculate the required electromagnetic losses as follows:

$$P_{\mathrm{cu1}} = mR_1 I_1^1 \quad \text{(stator copper losses)}, \tag{8}$$

$$P_m = mR_m I_m^2 \quad \text{(stator core losses)}, \tag{9}$$

$$P_{\mathrm{cu2}} = mR_2 I_2^2 \quad \text{(rotor copper losses)}, \tag{10}$$

where m is the phase number of the motor (in our case $m = 3$). Formulae (8)–(10) are used with the values for the phase currents computed by

$$I_1 = \frac{U_1(Z_m + Z_2)}{Z_{1\sigma}Z_m + Z_{1\sigma}Z_2 + Z_mZ_2}, \tag{11}$$

$$I_2 = \frac{U_1 Z_m}{Z_{1\sigma}Z_m + Z_{1\sigma}Z_2 + Z_mZ_2}, \tag{12}$$

$$I_m = \frac{U_1 Z_2}{Z_{1\sigma}Z_m + Z_{1\sigma}Z_2 + Z_mZ_2}, \tag{13}$$

where $Z_{1\sigma}$, Z_m and Z_2 are the phase impedance of stator, magnetising and rotor circuit, respectively

$$Z_{1\sigma} = R_1 + jX_{1\sigma}, \quad Z_2 = R_2/s + jX_{2\sigma}, \quad Z_m = R_m + jX_m. \tag{14}$$

Finally, the leakage reactances $X_{1\sigma}$, $X_{2\sigma}$ and X_m entering (14) are computed by using the following formulae

$$X_{1\sigma} = 2\pi f l_1, \quad X_{2\sigma} = 2\pi f l_2, \quad X_m = 2\pi f l_m, \tag{15}$$

where l_i, $i = 1, 2, 3$ are leakage inductances of stator and rotor, and the magnetised inductance, respectively. The values of these parameters are assigned when the motor is designed, and specific values for the motor analysed in this paper are given in Table 1 of the Appendix A.

Our next task is to evaluate heat transfer mechanism parameters. All three main transfer mechanisms, conduction, radiation, and convection, are involved in the heat exchange in TEFC-type motors.

Table 1
Computational results using the developed thermal model and their comparisons with experimental results

f (Hz)	5	10	15	30	40	50	75	100
M (Nm)	2.5	2.5	2.5	2.5	2.5	2.5	2.5	2.5
V (V)	32	48.5	68	128	153.6	208.7	234	308
s	0.12	0.066	0.035	0.022	0.018	0.015	0.017	0.033
T_{measured} (K)	75.23	60.54	53.36	46.33	44.11	42.29	36.59	20.05
$T_{\text{calculated}}$ (K)	69.11	55.91	50.51	47.83	45.44	45.10	37.65	22.21
ϵ (K)	6.12	4.63	2.85	1.50	1.33	1.07	1.06	1.03
$\epsilon\%$	8.14	7.65	5.35	3.29	3.02	2.52	2.73	5.17

2.2. Heat transfer in induction motors via conduction and radiation

In the solid parts of motors, such as the rotor and stator, heat is typically transferred by conduction. Hence, for these parts we use the standard Fourier's law to connect the heat flux and the temperature gradient:

$$\mathbf{q} = -k\nabla T. \tag{16}$$

In Table 3 of Appendix A we list the values of the thermal conductivity coefficient for the materials of interest.

A part of heat in induction motors is transferred by radiation. The actual amount of energy transferred in the form of electromagnetic waves depends not only on the emissivity properties of the part of the motor under consideration, but also on the temperature itself in a strongly non-linear way. Due to a temperature difference between the motor surface and the ambient temperature, the heat will be radiated out from the whole of the motor surface, and the energy radiated can be evaluated according to the Stefan–Boltzmann law of radiation (e.g., [19]):

$$Q = \epsilon\sigma T^4 A\,\Delta t, \tag{17}$$

where A is the surface area of the motor under consideration, ϵ is the emissivity coefficient, and $\sigma = 5.67 \times 10^{-8}$ W/m^2 K^4 is the Stefan–Boltzmann constant. In the notation used before $C_{\text{cons}} = \epsilon\sigma$. In Table 4 of the Appendix A we provide the values of ϵ for the materials of interest in this paper. In the most general setting, accounting for electromagnetic radiation should lead to an integro-differential due to the fact that electromagnetic radiation propagates in all directions. However, if the diffusion approximation is used the discussion on heat exchange can be reduced formally to conductive Fourier's law $\mathbf{q} = -k_{\text{r}}\nabla T$, but with strongly temperature-dependent radiative coefficient, $k_{\text{r}} = 16\sigma/(3\kappa_{\text{r}})$, where κ_{r} is the Rossseland mean absorption coefficient (e.g., [8]). In [18] it was pointed out that a simpler model for the radiation heat transfer can often be used, e.g. $q = h_{\text{r}}(T - T_{\text{ext}})$, due to the fact that the radiation transfer coefficient, h_{r}, does not vary substantially for typical operating temperatures of electric induction motors. As we shall discuss in the next section, a similar expression can also be used for the convection, but the estimation of the heat transfer coefficient in that case is conducted in a quite different manner. Let us consider these issues in detail.

2.3. Heat transfer in induction motors via conduction

The motor analysed in this paper as a case study example is enclosed with an external fan. This will cause force convection on the frame of the motor where the air does not flow on its own but it is rather pushed (see Fig. 3). There are other parts of the motor where convection models for the energy transfer are used, in particular for the heat transfer in the air gap, from shafts, from the rotor, shaft ends and magnetic bearings (the later three can be modelled as heat transfer from rotating discs), in the cooling duct, and in the end-winding space. The expression for the flux of such forced convection is given in the form

$$q = h(T - T_{\text{ext}}), \tag{18}$$

where, as before, T is the surface temperature and T_{ext} in this case is the temperature of the air/fluid. Although the evaluation of h in (18) can be conducted by using known tools [8], in each of the mentioned cases the evaluation of the heat transfer coefficient is a quite involved process. In what follows we concentrate on the evaluation procedure for h in the case of heat transfer from the frame to the external environment. It is generally agreed that this is the most important thermal effect (e.g., [17, p. 95]). The procedure discussed below follows the ideas along the lines discussed in [17,23].

In evaluating the convection coefficient h for the heat transfer from the frame to the external environment, we must take into account the dissipation from the fins of the frame (denoted further by h_a) and the dissipation from the surface between the fins (denoted further by h_l). The evaluation of these coefficients is complex, and in the general case the values of these coefficients vary depending on (a) the spatial position (due to the airflow losses on the frame), and (b) the airflow characteristics provided by the external fan. We describe here a method for calculating the forced convection coefficient depending on the Reynolds number:

$$Re = V_{\text{a}} F_l / \kappa \tag{19}$$

where V_{a} is the airflow velocity at beginning of the fins (it is known that this velocity is approximately 70% of the peripheral fan speed, obtained from experimental results), F_l is the axial length of the fins, and κ is the kinematic viscosity of the air. The fins of the analysed squirrel-cage induction motor are 20 mm in depth. The number of the fins is 36. Their average width is 140 mm, and the distance between two fins is 10 mm. In the current analysis the thickness of a fin, which is 3mm, does not play any role. Now, our focus is on the general procedure for the evaluation of h_a

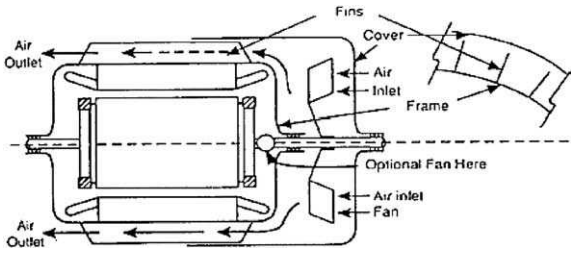

Fig. 3. Cooling airflow paths of the TEFC induction motor.

and h_l which requires an estimate for (19), after which the procedure follows one of the following two directions.

2.3.1. Laminar airflow case ($Re < 7 \times 10^4$)

In this case we define the quantity

$$H' = \frac{0.7(Re)^{0.5}[1 - 0.12(F_h/F_w)^{1/3}]K}{F_l}, \tag{20}$$

where F_w is the distance between two fins and F_h is the height of the fins, and K is the thermal conductivity of the air. Then, we calculate the convection coefficient related to the dissipation from the fins of the frame as follows:

$$h_a = H'[1 - 0.02(F_h/F_w)], \tag{21}$$

and the value of convection coefficient related to the dissipation from the surface between the fins as

$$h_l = \frac{0.7(Re)^{0.5}[1 - 0.35(F_h/F_w)^{1/3}]K}{F_l}. \tag{22}$$

2.3.2. Turbulent airflow case ($Re < 7 \times 10^4$)

In this case, H' is calculated as

$$H' = \frac{0.035(Re)^{0.6}[1 - 0.09(F_h/F_w)^{0.5}]K}{F_l}. \tag{23}$$

By using the value (23), h_a is then calculated according to formula (21), while for the calculation of h_l we use the following formula

$$h_l = \frac{0.03(Re)^{0.8}[1 - 0.23(F_h/F_w)^{0.5}]K}{F_l}. \tag{24}$$

Finally, we note that for the free convection coefficient we use the following formula (e.g., [16])

$$h_{\text{free}} = 6.5 + 0.05(T - T_{\text{ext}}). \tag{25}$$

Now, we are in a position to describe the main steps of the computational procedure.

3. Main steps of the finite-element-based computational procedure

The model described in Section 2 has been implemented by using the finite element methodology allowing us to deal with complicated geometries of electric motors and to account for a nonlinear character of the model. Basic implementation has been completed in a MATLAB-based finite element package FEMLAB. The results reported here focus on a two-dimensional implementation of the code.

1. *Constructing the geometric model of the induction motor.* The specific geometric sizes considered in this paper are based on the 1.5 KW, 2 poles, small size TEFC standard induction motor. This motor has been used in all our experimental work. The geometric model needed as an input to the finite element analysis has been created by using CAD tools. We combine a set of primitive solid objects and lines, arcs, and rational Bézier curves in order to produce a two-dimensional geometric model of motor. Fig. 4 shows all basic components of the axial cross-section of the motor. The numbering system in Fig. 4 corresponds to that of Fig. 1 where the complete structure of the TEFC squirrel-cage induction motor is given.
2. *Sub-domain specifications.* When the geometry is specified, we have to deal with a number of different regions of the motor where coefficients of the model should be specified. In fact, for typical computational experiments performed for the induction motors such as those analysed in this paper we need to deal with nineteen sub-domains, corresponding to the rotor part of the motor, end winding, fan-side bearing, etc. Coefficients and parameters used for one of such sub-domains, the stator part, are given in Table 5 of Appendix A.
3. *Discretisation procedure.* The computational geometry constructed and specified in the previous steps is partitioned into triangles, or mesh elements, and the refinement technique is used to ensure the required accuracy is achieved. As an example, we provide a typical partition of the axial cross-section of the motor with 8008 elements (Fig. 5).
4. *Solution of the problem and the visualisation procedure.* The problem is solved based on its variational formulation on different grids constructed with the refinement technique. In steady state situations a default plot is displayed. The result of computations of temperature distribution in the axial cross-section of the motor, as specified in Section 2, is given in Fig. 6. Sampling of the time-dependent solutions can also be performed in a user-friendly manner, as we explain below.

In the transient regime, which precedes the steady-state distribution of the temperature, the user is allowed to sample the calculated temperature. In particular, for typical operating conditions of the electric motor we deal with steady-state conditions are achieved in about one hour of operation. This has been also confirmed by experimental results discussed in the next sections. The user can set the time step and the sampling of the temperature distributions according to the

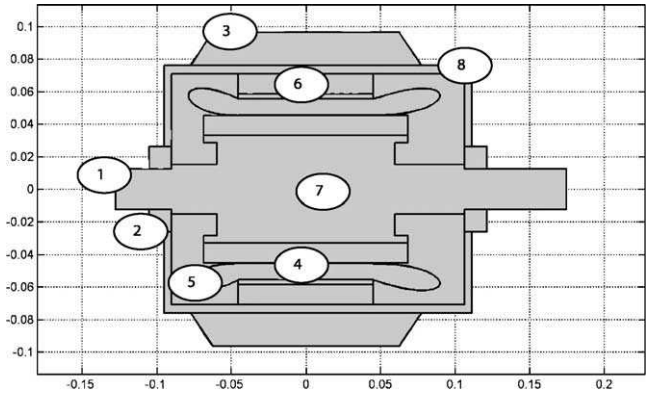

Fig. 4. The axial cross-section geometric configuration of the motor (dimensions are given in meters).

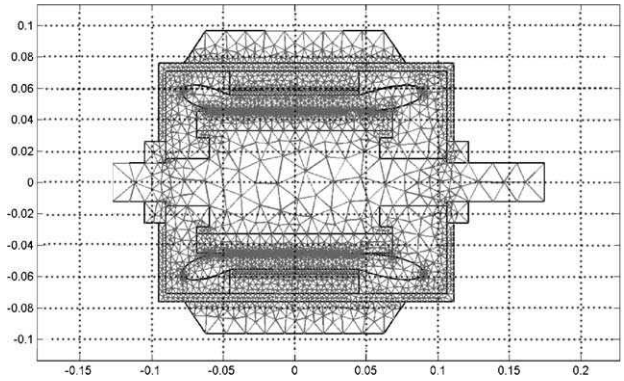

Fig. 5. Finite element discretisation—grid generation.

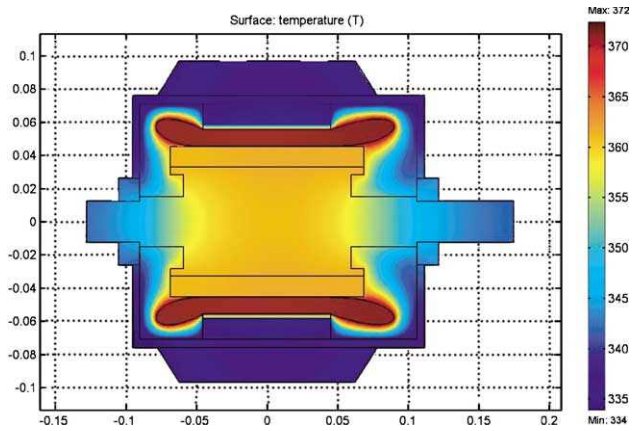

Fig. 6. Typical temperature distribution in the axial cross-section of the motor.

following rule: $t_0 : t_{\text{step}} : t_{\text{final}}$, e.g. the 0:100:10,000 setting has been used for our computational results (in Fig. 6 the temperature distribution is given at the last moment of observation), meaning that starting from the initial conditions we have sampled the solution every 100 s during 10,000 s of observation.

By analysing the temperature distribution in the axial cross-section presented in Fig. 6, it is clearly seen that the highest temperature occurs in the end winding area. This area is the most sensitive to possible thermal damages, and therefore we use this area as a benchmark example for the validation of the model.

In the next section we present our experimental setup that has been used for the model validation. The equipment allows us to generate data for temperature measurements in different parts of the motor under different operating conditions, and therefore to test the performance of the model described in Sections 2 and 3.

4. Experimental validation of the model

The experimental setup used for the model validation is presented in Fig. 7. There are nine temperature sensors (PT 1000) fixed inside the motor, provided by the control group at the R&D Department, Danfoss Drives (a 1.5 KW, 2 poles, small size TEFC standard induction motor). These temperature sensors are placed on the (fan side) bearing, end winding (inside and outside), air gap and frame (fin and between fins) areas. One sensor is put outside and is used to measure the ambient temperature. A switch box controls the working status of these sensors. To achieve a high accuracy of measurements, the sampling timer has been set to 3.5 s and all the data measured have been recorded in a computer.

As seen in Fig. 8, the motor was put inside a cage due to safety reasons. The apparatus was set to replicate the practical working situations of an induction motor, which is used to drive a load on the shaft. A frequency converter serves as an interface that connects the power supply and the motor in order to achieve control of the motor. The frequency converter can change the frequency input to the motor, as well as the power input. These input parameters can be detected by the frequency converter simultaneously. The torque on the motor shaft can be adjusted by an external equipment (the torque equipment) that is also shown in Fig. 8. The torque equipment, which is connected to the motor, can determine the current data of torque and detect the rotor speed in rpm. From the interfaces of the equipment described we can read the local operating data. The sampled results of the measurements are shown in Fig. 9. The temperature rise is given in a case where the motor is operated with a constant load and the input frequency changed from 75 to 50 Hz, then to 30 Hz, and finally to 15 Hz, as represented by four distinct regions in Fig. 9. It is also clearly seen that the temperature profiles vary substantially between different regions of the motor. In a similar way, we generated data for other operating conditions, and the obtained experimental results have been used in the model validation procedure.

The accuracy of the thermal model described in Sections 2 and 3 has been evaluated by comparing the results obtained numerically with the model and those obtained by the practical measurements in the corresponding conditions. It is known, that in most practical situations the

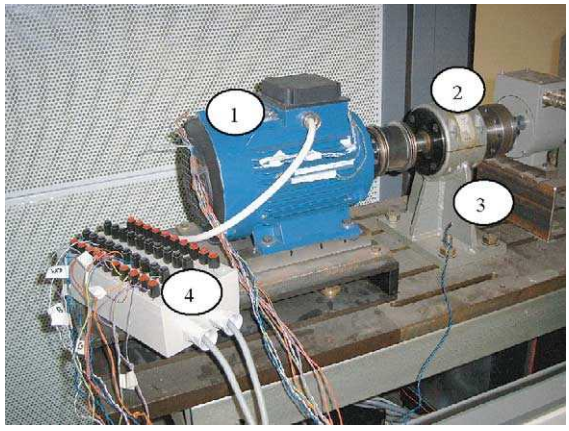

Fig. 7. The experimental setup for temperature sampling. (1) Motor; (2) load on the shaft; (3) outside sensor; (4) switch box.

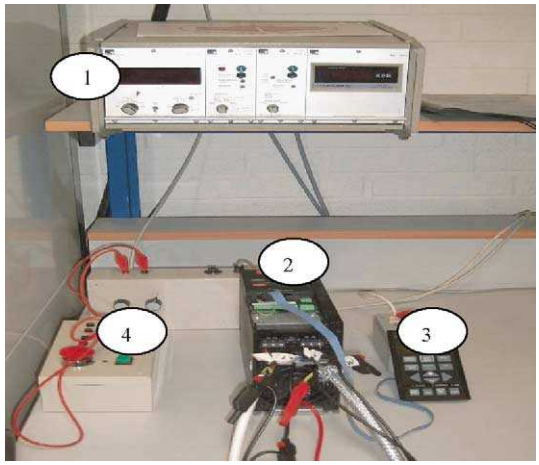

Fig. 8. Torque equipment used in the experiments and the frequency converter. (1) Display equipment; (2) frequency converter; (3) control panel; (4) torque equipment.

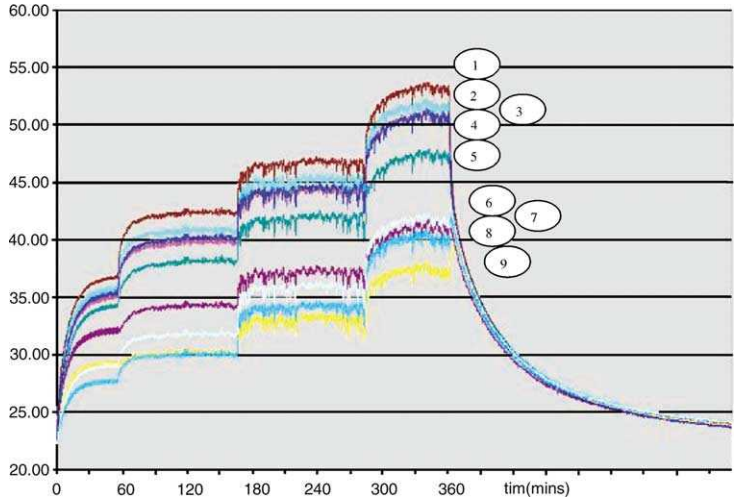

Fig. 9. Temperature rise plots produced for different frequencies of the motor 75, 50, 30, and 15 Hz and torque 2.5 N m. (1) "External" end winding; (2) fan-side "external" end winding; (3) "internal" end winding; (4) fan-side "internal" end winding; (5) bearing; (6) fan-side bearing; (7) air gap; (8) frame; (9) fins of the frame.

error of a usable thermal model should be less than 10% [7]. We have used a range of different operating parameters, and recorded the measured temperature rise in the end-winding area. These measurements are denoted here by T_{measured}. We have applied the same operating conditions as an input to the develop thermal model, and recorded the computed data for the end winding area. The results are denoted here by $T_{\text{calculated}}$. Comparisons are given in Table 1.

In this table by ε we denote the absolute error that is the absolute values of the difference between $T_{\text{calculated}}$ and T_{measured}, and by $\varepsilon\%$ we denote the relative error calculated by the formula:

$$\epsilon\% = \epsilon \times 100\%/T_{\text{measured}}. \tag{26}$$

The results clearly demonstrate that the errors of the developed computational model are less than 10% over a wide range of operating conditions.

5. Model-based control for preventing thermal damages of electric motors

The developed model can be applied to predict and to help avoiding thermal damages of induction motors working under a range of operating conditions. In this section, we show how the developed model can be applied to perform this function.

We consider the following case study example. A user wants to apply a 1.5 KW, 2 poles, small size TEFC standard induction motor with insulation class B (this class has the allowable temperature threshold at 393 K) for a certain period of time. According to the requirements of the load, the specified input parameters are: frequency is at 30 Hz, phase voltage is at 133 V, and the torque on the shaft is at 10 Nm. Based on this information, we can calculate auxiliary parameters we need, in particular the slip (see (6)) which is 0.14. We need to determine for how long the motor can operate under the given condition without exceeding the specified temperature limit. To solve this and similar problems we have developed a program in SIMULINK that uses our thermal model as an input. In Fig. 10 we show schematically a SIMULINK diagram used to monitor the thermal operation of the motor. In the diagram, the three blocks on the left are used to define the operating conditions/parameters sent as an input to the thermal model. The output from the developed model in this case is the highest temperature inside the motor (Fig. 11). In the case considered in this paper it is the end-winding temperature. This temperature is then compared to the thermal limit trip specified by the user. The thermal limit value is kept in the T_{limit} block. If the result of this comparison shows that the temperature in the motor is higher than the limit temperature, the warning block will be activated. The thermal process under the operation can be observed by using the display block. Under the given conditions, the temperature in the end winding will hit the 393 K limit after 3200 s of the motor operation, which means that the motor

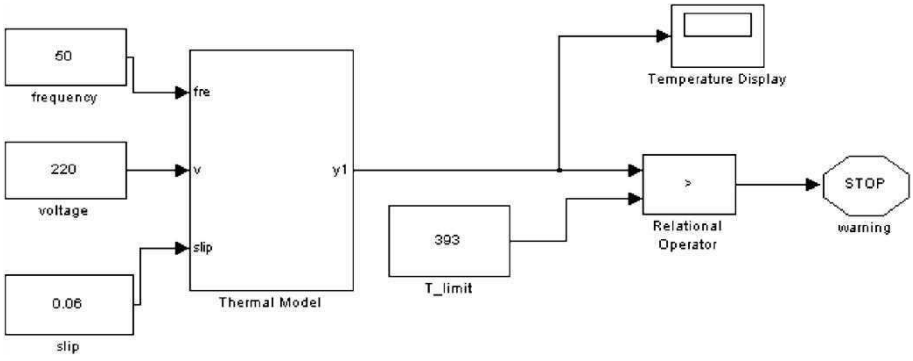

Fig. 10. Schematic diagram showing the thermal model as an input to a control loop designed in SIMULINK in order to control thermal processes of motors.

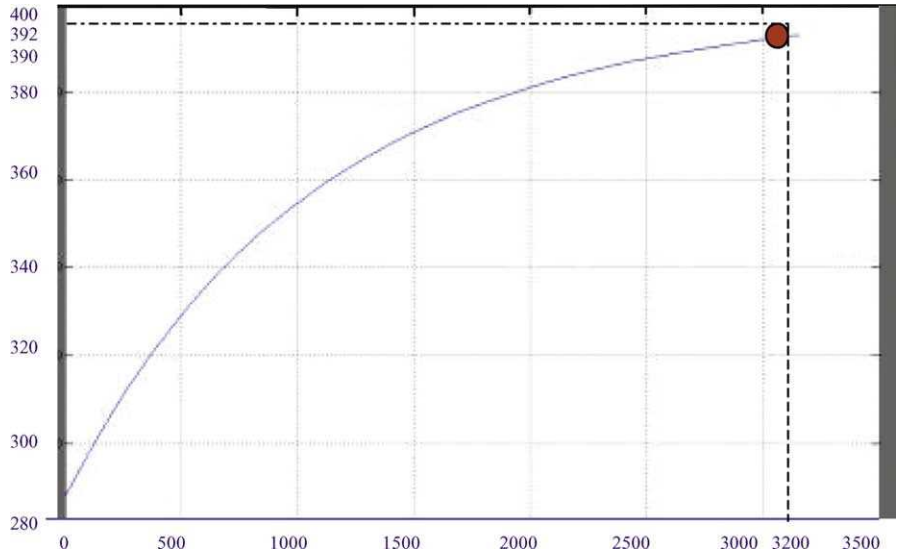

Fig. 11. Typical output from SIMULINK: temperature as a function of time in the end-winding area.

should be operational for less than one hour to avoid overheating. With simple modifications, and combined with the SIMULINK program, the developed thermal model can perform simulation and control functions based on a wide range of practical requirements.

6. Concluding remarks

In this paper we have proposed a general approach to modelling temperature rise phenomena in electric induction motors, and demonstrated the effectiveness of this approach by comparisons of the modelling results with the results of experimental measurements. As a case study example, the analysis of TEFC induction motors operating under different voltage supplies and loading conditions has been presented, and an application example, combining the developed tool with a SIMULINK-based code, has been given.

Appendix A

Motor typical parameters are listed in Table 2. Thermal conductivity coefficients of the main relevant materials used in the computations are given in Table 3. The emissivities of the materials used in the calculations ($e_{\text{blackbody}} = 1$) are given in Table 4. Typical parameters used for one of the 19 sub-domains used in our experiments, namely for the stator part, are given in Table 5. In this case, the iron losses constitute a major part of heat sources. Convection and radiation coefficients, as well as external and ambient temperatures were set to zero in this case (see (4)).

Table 2
Nominal parameters of the motor used in the experiment

Parameters	Value
Power	1.5 kW
Phase angle	0.79
Mass	13.5 kg
Rotor speed	1400 rpm
Phase number	3
Stator inductance	0.01598 H
Magnetising inductance	0.2972 H
Rotor inductance	0.01182 H
Voltage	380–415 V
Current	3.55 A
Frequency	50 Hz
Pole pair number	2
Stator resistance	6.509 Ω
Magnetising resistance	2200 Ω
Rotor resistance	4.512 Ω

Table 3
Thermal conductivity coefficients (in W/m K) for different parts of the induction motor

Material	k
Iron	58
Plastic	0.2
Aluminum	222
Steel	35
Copper	388

Table 4
Emissivity coefficients for different parts of the motor

Material	ϵ
Cast iron (rough)	0.97
Forging iron (polished)	0.29
Forging iron (oxidised)	0.95
Aluminum	0.08

Table 5
Basic parameters and coefficients in the stator core sub-domain

PDE coefficients	Value/expression
Density	7850 (kg/m^3)
Thermal conductivity	58 (W/m K)
Heat capacity	480 (J/kg K)
Heat sources	$3R_mI_m^2$

References

[1] A.F. Armor, M.V.K. Chari, Heat flow in the stator core of large turbine-generators by the method of 3D finite elements, IEEE Trans. Power Apparatus Syst. PAZ-95 (5) (1976) 1648–1656.
[2] R. Beguenane, M.E.H. Benbouzid, Induction motors thermal monitoring by means of rotor resistance identification, IEEE Trans. Energy Convers. 14 (3) (1999) 566–570.
[3] A. Bousbaine, Thermal modelling of induction motors based on accurate loss density distribution, Electr. Machines Power Syst. 27 (1999) 311–324.
[4] J.T. Boys, M.J. Miles, Empirical thermal model for inverter-driven cage induction machines, IEE Proc. Electr. Power Appl. 141 (6) (1994) 360–372.
[5] T.F. Chan, A method to determine the temperature rise of induction motors, Int. J. Electr. Engng. Edu. 27 (1990) 45–52.
[6] P. Dokopoulos, J. Xypteras, Analytische berechnug der transienten temperaturverteilung in elektrischen maschinen, etzArchiv 6 (2) (1984) 23–76.
[7] S.L. Ho, W.N. Fu, Analysis of indirect temperature-rise tests of induction machines using time stepping FEM, IEEE Trans. Energy Convers. 16 (1) (2001) 55–60.
[8] F. Kreith (Ed.), CRC Handbook of Mechanical Engineering, CRC Press, 1998.
[9] G. Kylander, Thermal modeling of small cage induction motors, Doctoral thesis, Göteborg, Sweden, Chalmers University of Technology, School of Electrical and Computer Engineering, Technical Report No. 265, February 1995.
[10] X. Luo et al., Multiple coupled circuit modeling of induction motors, IEEE Trans. Indust. Appl. 31 (2) (1995) 311–318.
[11] R.V.N. Melnik, A.J. Roberts, K.A. Thomas, Phase transitions in SMA with hyperbolic heat conduction and differential-algebraic models, Comput. Mech. 29 (2002) 16–26.
[12] H.M.B. Metwally, Loadless full load temperature rise test for three phase induction motors, Energy Convers. Mgmt. 42 (2001) 519–528.
[13] A. Mihalcea, B. Szabados, J. Hoolboom, Determining total losses and temperature rise in induction motors using equivalent loading methods, IEEE Trans. Energy Convers. 16 (3) (2001) 214–219.
[14] S.C. Mukhoppadhyay, S.K. Pal, Temperature analysis of induction motors using a hybrid thermal model with distributed heat sources, J. Appl. Phys. 83 (11) (1998) 6368–6370.
[15] M.N. Ozisik, Heat Conduction, second ed., John Wiley & Sons, 1993.
[16] R. Richter, Elektrische Maschinen. Bd. 4 Die Induktionsmaschinen, Birkhäuser Verlag, Basel, 1954.
[17] J.L. Romo, M.B. Adrian, Prediction of internal temperature in three-phase induction motors with electronic speed control, Electr. Power Syst. Res. 45 (1998) 91–99.
[18] J. Saari, Thermal model of high-speed induction machines, Acta Polytichnica Scandinavia, Electrical Engineering Series, No. 82, Helsinki, 1995.
[19] R. Siegel, J.R. Howell, Thermal radiation heat transfer, third ed., Hemisphere Publ. Co., Washington, 1992.
[20] C.E. Tindall, S. Brankin, Loss-at-source thermal modeling in salient pole alternators using 3D finite difference technique, IEEE Trans. Magn. 24 (1) (1988) 278–281.
[21] H.A. Toliyat, T.A. Lipo, J.C. White, Analysis of a concentrated winding induction machine for adjustable speed drive applications, IEEE Trans. Energy Convers. 6 (4) (1991) 679–692.
[22] S.E. Zocholl, Induction motors (Part 1: Analysis; Part 2: Protection), Schweitzer Engineering Labs Technical Reports (http://www.selinc.com/techpprs.htm), Pullman, WA, 2002.
[23] A. Woolfolk, Specifying filters for forced convection cooling, Electron. Cooling 1 (2) (1995) 20–23.